




# Effect of the Fe<sub>2</sub>O<sub>3</sub> addition on the elastic and gamma-ray shielding features of bismuth sodium-borate glass system

Haifa A. Al-Yousef<sup>1</sup>, Mohammed Alotiby<sup>2,\*</sup>, M. Y. Hanfi<sup>3,4</sup>, B. M. Alotaibi<sup>1</sup>, K. A. Mahmoud<sup>3,4</sup>, M. I. Sayyed<sup>5,6,\*</sup> , and Y. Al-Hadeethi<sup>7</sup>

<sup>1</sup>Department of Physics, College of Science, Princess Nourah Bint Abdulrahman University, Riyadh, Saudi Arabia

<sup>2</sup>King Abdulaziz City for Science and Technology, Riyadh, Saudi Arabia

<sup>3</sup>Ural Federal University, Mira St., 19, Yekaterinburg, Russia 62002

<sup>4</sup>Nuclear Materials Authority, El Maadi, Cairo, Egypt

<sup>5</sup>Department of Physics, Faculty of Science, Isra University, Amman 11622, Jordan

<sup>6</sup>Department of Nuclear Medicine Research, Institute for Research and Medical Consultations, Imam Abdulrahman Bin Faisal University, Dammam 31441, Saudi Arabia

<sup>7</sup>Department of Physics, Faculty of Science, King Abdulaziz University, Jeddah 21589, Saudi Arabia

Received: 6 December 2020

Accepted: 24 January 2021

Published online:

23 February 2021

© The Author(s), under exclusive licence to Springer Science+Business Media, LLC part of Springer Nature 2021

## ABSTRACT

The elastic properties were predicted for four glass samples with chemical compositions  $x\text{Fe}_2\text{O}_3 + (25 - x)\text{Bi}_2\text{O}_3 + 75\text{Na}_2\text{B}_4\text{O}_7$ , where  $x = 5, 10, 15$ , and  $20$  mol%. The studied glass samples' molar volume and molecular weight were studied based on the chemical composition and the sample density. Moreover, the Makishima–Mackenzie model was applied to predict the studied glass samples' elastic properties. The elastic moduli were observed to increase gradually with the Fe<sub>2</sub>O<sub>3</sub> insertion ratio and the packing density increase. The elastic moduli ranged between 57.67–85.29 GPa, 33.47–65.49 GPa, 23.77–33.24 GPa, and 65.17–109.81 GPa for Young, Bulk, Shear, and Longitudinal moduli, respectively. Moreover, the Monte Carlo simulation code and XCOM software program were applied to predict the main shielding parameters, linear attenuation coefficient (LAC), and mass attenuation coefficient (MAC). The LAC varied between 2.138–0.197 cm<sup>-1</sup> and 0.946–0.186 cm<sup>-1</sup> for glass samples with 5 and 20 mol% of the Fe<sub>2</sub>O<sub>3</sub> content. Based on the simulated LAC, the half-value layer (HVL), mean free path (mfp), and the radiation protection efficiency (RPE) were estimated. The BXCOS software program was applied to predict the photon accumulation inside the studied glass samples (exposure buildup factor (EBF) and energy absorption buildup factor (EABF)).

Address correspondence to E-mail: mfofoty@kacst.edu.sa; mabualssayed@ut.edu.sa

## 1 Introduction

In the Nuclear Physics Sector, radiations are found in many different areas, including the industrial division, diagnosis, research labs, agricultural products irradiation, environmental application, and health applications. It is a challenge for a nuclear physicist to minimize the unfavorable influences of unsafe radiation. Gamma radiation is emitted from different sources, divided into natural sources such as cosmic radiation and human-made radiation such as the radiations emitted from nuclear medical machines [1]. In both cases, gamma radiations carry high amounts of energy; thus, gamma photons have high frequency and move at light speed. For these reasons, they are very dangerous and sometimes called ionizing radiations. They are deliberately or undeliberately lethal radiations [2–4]. Exposure to these harmful radiations unknowingly or knowingly for relatively long or short periods of time, but periodically, causes strong poisoning radiation and, in some cases, leads to death. The radiation protective materials must be used to avoid these hazards arising from radiation. The shielding materials are considered one of the most important precautionary methods that must be followed in any establishment that uses radiation, regardless of its nature or energy, to provide adequate protection [5–7]. For instance, using enormous concrete blocks around nuclear facilities is traditionally developed to protect the surrounding environment from radiation [8]. The apron is also used by people who work in the field of radiography in the medical fields, as well as for the patient during the radiation treatment process to reduce the effects of ionizing radiation [9]. Regardless of the material used in radiation protection, whether it is concrete, lead, or other traditional materials used for this purpose, all materials used must have a relatively high atomic number as well as a relatively high density, so it is not surprising to find that lead which has an atomic number of 82, and a density of about  $11.3 \text{ g cm}^{-3}$  is one of the most common materials used in radiation protection applications [10, 11]. Recent studies have shown that lead has many disadvantages; the most important is its toxicity and its heavy weight, which causes health problems in the spine of medical workers who wear the apron made of lead and opaque lead. Therefore, it is not possible to develop protective radiation glasses from lead [12]. Considering all these issues, investigators have been

trying to find alternative protection materials from the past years. Glass samples, especially those fabricated with heavy metal oxides, are known to offer sufficient gamma radiation protection [13–16]. Novel glass systems for gamma-ray attenuation applications continue to be prepared and examined by different researchers [17–21].

The new generations of glasses shielding materials are fabricated, particularly by incorporating some heavy metal oxides such as  $\text{Bi}_2\text{O}_3$ ,  $\text{WO}_3$ ,  $\text{BaO}$ ... and so on to provide almost the same function as lead or lead composite attenuating the photons [22]. But so far, there has been no glass system capable of performing the same role that leads to radiation protection. Therefore, studies are developing novel glass systems that can attenuate more radiation and try to find certain glass systems with the same efficiency as lead [21–25].

To reach this goal, and before carrying out any experimental work, glass samples' ability must be examined in terms of radiation protection theoretically or by using specific simulation programs. In the simulation, we create the same conditions for the practical experiment in the laboratory, and through the obtained results, we can estimate the possibility of using the examined glass as a protective material against radiation and then actually start the practical experiment. In other words, the goal of the simulation is to save time and effort to study the possibility of developing a specific glass system as a protective material for radiation and based on the simulated results. We can change the glass's chemical composition to obtain better radiation protection results [26, 27]. The present work novelty has pointed to predicting the elastic properties for the investigated glass samples using the Makishima–Mackenzie model. Moreover, the Monte Carlo simulation code MCNP-5 has been used to estimate the mean track length of the projected gamma photons inside the studied glass samples. Based on the simulated mean track length, other shielding properties such as the mean free path (mfp), half-value layer (HVL), radiation protection efficiency (RPE), and the transmission factor (TF) have been calculated. Furthermore, the BXCOS has been used to obtain the buildup factors for exposure (EBF) and energy absorption (EABF) through the G-P fitting method in ANSI.

## 2 Materials and methods

Four glass samples consisting of  $x\text{Fe}_2\text{O}_3-(25-x)\text{Bi}_2\text{O}_3-75\text{Na}_2\text{B}_4\text{O}_7$  have been produced by Al-hajry et al., 2005. The density, optical, and dielectric properties were measured and studied in ref [28]. Based on the measured density and the chemical composition of the studied samples, the molecular weight  $M_W$  and molar volume  $V_M$  were calculated using Eqs. 1 and 2.

$$M_W(\text{gmol}^{-1}) = \sum_i X_i(M_w)_i \quad (1)$$

$$V_M(\text{cm}^3\text{mol}^{-1}) = \frac{M_W}{\rho_{\text{glass}}} \quad (2)$$

where  $X_i$  and  $(M_w)_i$  refer to the molar fraction and the molecular weight of the constituting compounds, respectively.

### 2.1 Elastic properties

Makishima–Mackenzie model has been used to estimate the elastic properties of the studied  $\text{Fe}_2\text{O}_3\text{–Bi}_2\text{O}_3\text{–Na}_2\text{B}_4\text{O}_7$  (FBN) glass system. Firstly, the Makishima–Mackenzie model based on the energy needed to break the chemical bond between molecules in the studied glass (dissociation energy  $G_i$ ) and the ionic ( $R$ ) radius of each element in the glass system [29].

$$G_i(\text{kJcm}^{-3}) = \sum_i G_i X_i \quad (3)$$

$G_i$  represents the dissociation energy of  $i$ th constituent in the FBN glass samples. Based on the ionic radius values and the coordination number of the metal and oxygen atoms constituting the glass system, the packing factor  $V_i$  was calculated according to Eq. 4 [29].

$$V_i(\text{cm}^3\text{mol}^{-1}) = \frac{4\pi}{3} N_A (XR_A^3 + YR_o^3) \quad (4)$$

where  $N_A$ ,  $R_A$ ,  $R_o$ ,  $X$ , and  $Y$  denote Avogadro's number, the metal ionic radius, oxygen ionic radius, the number of metal atoms, and oxygen atoms, respectively. After that, the packing density of the investigated samples was calculated based on the packing factor, as illustrated in Eq. 5.

$$V_t = \frac{\rho}{M_w} \sum_i V_i X_i \quad (5)$$

The elastic moduli, Poisson ratio ( $\sigma$ ), and the microhardness ( $H$ ) corresponding to the studied glass samples were calculated, taking into consideration the predicted values of  $G_i$  and  $V_t$ , as illustrated in Eqs. (6–11) [30, 31].

$$E = 2V_t G \quad (6)$$

$$B = 1.2V_t E \quad (7)$$

$$S = \frac{3EB}{(9B - E)} \quad (8)$$

$$L = B + \frac{3}{4}S \quad (9)$$

$$\sigma = 0.5 - \frac{1}{7.2}V_t \quad (10)$$

$$H = \frac{(1 - 2\sigma)}{6(1 + \sigma)} \quad (11)$$

### 2.2 Radiation shielding features

The MCNP-5 has been used to study the gamma-ray shielding ability of FBN glasses. An input file containing the required information about the geometry has been implemented to predict the gamma-ray shielding properties, as shown in Fig. 1. A lead cylinder with a thickness of 5 cm shielded the detector, glass samples, and the gamma source from any external interference. The source was anticipated to emit  $10^6$  photons per minute in the + Z direction. Several gamma sources,  $^{166}\text{Ho}$  with energy 0.184, 0.280, and 0.710 MeV,  $^{137}\text{Cs}$  with an energy of 0.662, and  $^{60}\text{Co}$  with energies of 1.173 and 1.332 MeV, have been selected in the present study.

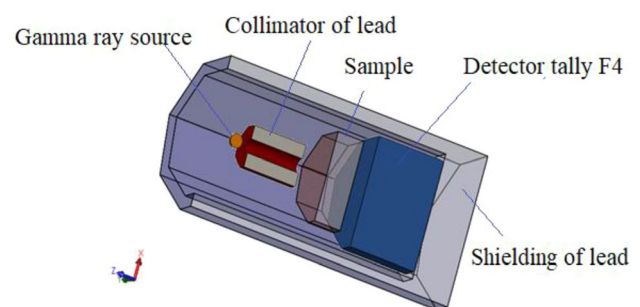


**Fig. 1** The geometry setup of the MCNP-5 simulation used for the prediction of the MAC for the FBN samples

The emitted photons were collimated using a lead collimator measuring 10 cm in height, 7 cm in diameter, and 2 cm in central diameter. Then the collimated photons passed onto the FBN glass that was positioned in the middle between the lead collimator and the detector. The chemical composition, density, and molar weight of the FBN glasses are displayed in Table 1. The detector was assumed to be an F4 tally to calculate the incoming photons' average track length in the FBN glasses. The simulation was then finished, and the output reported that less than 1% was the relative error for the average track length measurement [32].

The linear attenuation coefficient (LAC,  $\mu$ ) is estimated on the basis of the mean track length recorded in MCNP-5 and presented. The mass attenuation coefficient (MAC,  $\mu_m$ ) is used to estimate the glass's attenuation per unit density and can be represented by Eq. (12) [33].

$$\mu_m = \frac{\mu(\text{cm}^{-1})}{\rho(\text{gcm}^{-3})} \text{ or } \mu_m = \sum_i w_i (\mu_m)_i \tag{12}$$

where  $w_i$  and  $(\mu_m)_i$  are the fractional weight and the mass attenuation coefficient of the element's  $i$ th constituents, respectively.

The transmission factor (TF) is also applied for the prediction of the proportion of gamma photons that can be transmitted with a known thickness and can be calculated by Eq. (13).

$$\text{TF} = \frac{I}{I_0} = \exp(-\mu x) \tag{13}$$

The half-value layer (HVL) shows the thickness of the attenuator that can diminish the intensity of the incoming photon to half its starting value and can be calculated with Eq. (14) on the basis of the LAC values [34].

$$\text{HVL} = \frac{\ln(2)}{\mu(\text{cm}^{-1})} \tag{14}$$

The average distance between two subsequent collisions is the mean free path (MFP). As the MFP decreases, the number of interactions between the incoming photons and the atoms of the material increases, increasing the absorption and the attenuation. It is also possible to calculate MFP based on LAC values similar to HVL, as shown in Eq. (15).

$$\text{MFP} = \frac{1}{\mu(\text{cm}^{-1})} \tag{15}$$

In order to determine the values of other shielding factors, such as the effective atomic number ( $Z_{\text{eff}}$ ), equivalent atomic numbers ( $Z_{\text{eq}}$ ), exposure buildup factor (EBF), and energy absorption buildup factor (EABF), the BXCOSY program was utilized [35].

### 3 Results and discussion

#### 3.1 Elastic properties

The investigated FBN5-FBN20 glass samples' density has been measured experimentally, as mentioned previously by Al-hajry et al., 2005. The molecular weight ( $M_w$ ) and the molar volume ( $V_M$ ) of the studied glass samples were calculated according to Eqs. 2 and 3, listed in Table 1.  $\text{Bi}_2\text{O}_3$  by  $\text{Fe}_2\text{O}_3$  contents' replacement caused a decrease in the  $M_w$  calculated values between 151.8 and 105.54  $\text{g mol}^{-1}$  for glasses coded FBN5 with  $\text{Fe}_2\text{O}_3$  content 5 mol% and FBN20 with 20 mol % of  $\text{Fe}_2\text{O}_3$ , respectively. Table 1 also shows that both density and the molar  $V_M$  of the investigated glass samples decreased with increasing the  $\text{Fe}_2\text{O}_3$  substitution ratio. The studied glasses' density ranged between 3.757 and 3.587  $\text{g cm}^{-3}$ , increasing the  $\text{Fe}_2\text{O}_3$  content between 5 and 20 mol%

**Table 1** The chemical composition, density, and molecular weight of FBN glasses

Glass code	Chemical composition (mol%)			Density ( $\text{g cm}^{-3}$ )	Molecular weight ( $\text{g mol}^{-1}$ )	Molar volume ( $\text{cm}^3 \text{mol}^{-1}$ )
	$\text{Fe}_2\text{O}_3$	$\text{Bi}_2\text{O}_3$	$\text{Na}_2\text{B}_4\text{O}_7$			
FBN5	5	20	75	3.757	151.48	40.32
FBN10	10	15	75	3.706	136.17	36.74
FBN15	15	10	75	3.638	120.85	33.22
FBN20	20	5	75	3.587	105.54	29.42

due to the replacement of the  $\text{Bi}_2\text{O}_3$  with a high density ( $\rho = 8.9 \text{ g cm}^{-3}$ ) by  $\text{Fe}_2\text{O}_3$  with lower density ( $\rho = 5.24 \text{ g cm}^{-3}$ ). The  $V_M$  has the same trend as the glass density, decreased between 40.32 and 29.42  $\text{cm}^3 \text{ mol}^{-1}$ , raising the  $\text{Fe}_2\text{O}_3$  ratio between 5 and 20 mol%.

One of the present work's main targets is to evaluate the elastic properties of the investigated FBN5–FBN20 glass samples. The mathematical theoretical Makshima–Makinzi model was applied to achieve the mentioned aim based on the chemical composition, the ionic radius, and the dissociation energy of the constituting metal oxides. According to Eq. 3, the packing factor ( $V_i$ ) of the investigated glass samples was calculated for the glass constituting compound. The dissociation energies for each compound were calculated relying on the chemical interaction's enthalpy. After that, the  $V_i$  and the total dissociation energy ( $G_t$ ) have been calculated for the investigated glass; the predicted results are listed in Table 2. The variation of the  $V_i$  and  $G_t$  versus the  $\text{Fe}_2\text{O}_3$  ratio is illustrated in Fig. 2. It is clear that the packing factor of the investigated glass samples decreased from 19.50 to 18.83  $\text{cm}^3 \text{ mol}^{-1}$ , while the  $G_t$  increased from 59.62 to 66.66  $\text{kJ cm}^{-3}$ . The opposite trend comes out from replacement of  $\text{Bi}_2\text{O}_3$  ( $V_i = 26.1 \text{ cm}^3 \text{ mol}^{-1}$  and  $G_t = 31.6 \text{ kJ cm}^{-3}$ ) with  $\text{Fe}_2\text{O}_3$  ( $V_i = 21.6 \text{ cm}^3 \text{ mol}^{-1}$  and  $G_t = 78.5 \text{ kJ cm}^{-3}$ ). This can also indicate that, with increasing the  $\text{Fe}_2\text{O}_3$  substitution ratio, the Fe–O–Bi and Bi–O–Bi bonds have been broken, and new Fe–O–Fe bonds were created [28].

Based on the calculated  $V_i$  and  $G_t$  of the investigated glass samples, the elastic moduli Young, Shear, Bulk, and longitudinal were calculated as listed in Table 2. Figure 3 shows the elastic moduli variations versus the packing density of the investigated glass samples. The predicted results showed that the elastic moduli were directly increased with the  $V_t$

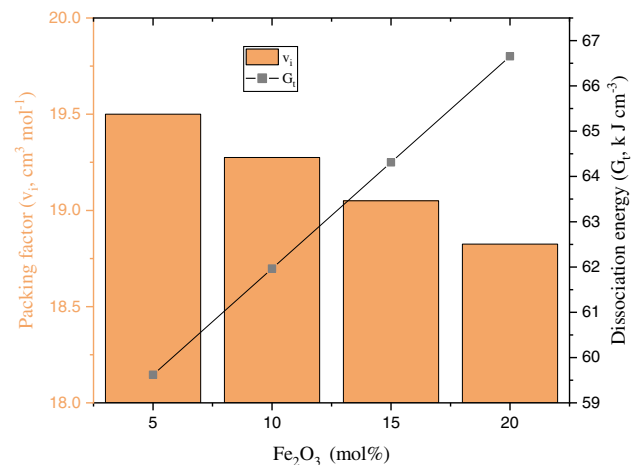


**Fig. 2** Variation of the packing factor ( $V_i$ ) and dissociation energy ( $G_t$ ) versus the  $\text{Fe}_2\text{O}_3$  substitution ratio

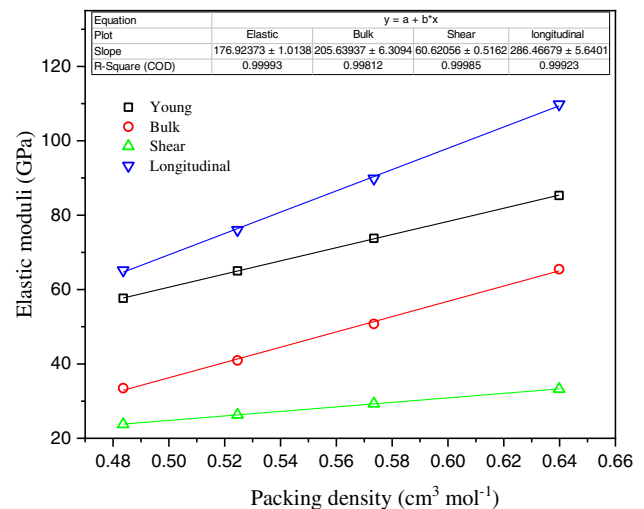


**Fig. 3** Variation of the elastic moduli versus the packing density of the fabricated glass samples

increase. The moduli have the following values 57.67–85.29 GPa, 33.47–65.49 GPa, 23.77–33.24 GPa, and 65.17–109.81 GPa for Young, Bulk, Shear, and

**Table 2** The packing factor ( $V_i$ ), packing density ( $V_t$ ), dissociation energy ( $G_t$ ), micro-hardness ( $H$ ), Poisson ratio ( $\mu$ ), and the elastic moduli Young ( $E$ ), Bulk ( $B$ ), Shear ( $S$ ), and longitudinal ( $L$ ) for the studied glass samples

	Elastic properties								
	$V_i$ ( $\text{cm}^3 \text{ mol}^{-1}$ )	$G_t$ ( $\text{kJ cm}^{-3}$ )	$V_t$ ( $\text{cm}^3 \text{ mol}^{-1}$ )	$E$ (GPa)	$B$ (GPa)	$S$ (GPa)	$\mu$	$H$ (GPa)	$L$ (GPa)
FBN5	19.50	59.62	0.48	57.67	33.47	23.77	0.21	4.55	65.17
FBN10	19.28	61.97	0.52	65.01	40.93	26.32	0.24	4.64	76.02
FBN15	19.05	64.31	0.57	73.76	50.76	29.32	0.26	4.73	89.85
FBN20	18.83	66.66	0.64	85.29	65.49	33.24	0.28	4.81	109.81

Longitudinal moduli when the packing density of the glass samples increased from 0.48 to 0.064 cm<sup>3</sup> mol<sup>-1</sup>.

The micro-hardness (*H*) and the Poisson’s ratio ( $\sigma$ ) were calculated relying on the elastic moduli’s predicted values. Figure 4 illustrates the variation of *H* and  $\sigma$  as a function of the Fe<sub>2</sub>O<sub>3</sub> insertion ratio. Figure 4 shows that the Poisson’s ratio increased from 0.21 to 0.28, while the *H* improved from 4.55 to 4.81 GPa, raising the Fe<sub>2</sub>O<sub>3</sub> insertion ratio from 5 to 20 mol%.

The currently predicted elastic moduli were compared to the previously performed similar glass samples, as shown in Table 3, to confirm the predicted values’ accuracy. Table 3 shows that the calculated values are comparable to the values reported by previous works [36–39].

### 3.2 Gamma-ray shielding properties

The shielding properties have been studied for the FBN glasses, where the MCNP-5 code was used to detect a few shielding parameters such as the linear attenuation coefficient (LAC), mass attenuation coefficient (MAC), transmission factor (TF), half-value layer (HVL), and mean free path (MFP). The LAC of the investigated FBN glasses was simulated and presented in Fig. 5. This exhibits the LAC depending on two main factors, which are incoming photon energy and the Fe<sub>2</sub>O<sub>3</sub> content in the FBN glasses. The highest values of LAC were observed at energy 0.184 MeV. The LAC values decreased from 2.14 cm<sup>-1</sup> for glass FBN5 to 1.24 cm<sup>-1</sup> for glass FBN20. Also, it decrease progressively with an

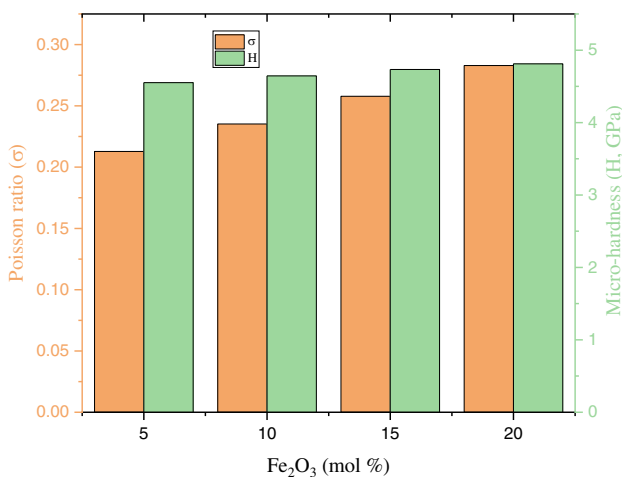
increase in the incoming photon energy. This decrease is due to the rapidly decreasing in the photoelectric effect, which leads to the predominance of the Compton scattering at roughly a few hundred keV. The cross-section of Compton scattering is proportional inversely to the incoming photon energy ( $\sigma_{com} \propto E^{-1}$ ) [40]. At high incoming photon energy (1.408 MeV), the lowest LAC values were achieved and reduced in-between 0.197 and 0.186 cm<sup>-1</sup> for FBN5 and FBN20 glasses, respectively.

The other factor that affects the LAC is the chemical composition of FBN glasses. With increasing the Fe<sub>2</sub>O<sub>3</sub> content in FBN glasses, the investigated glasses’ molecular weight increased associated with decreasing in the *Z*<sub>eff</sub> values of the FBN glasses. At a low Fe<sub>2</sub>O<sub>3</sub> insertion ratio (i.e., 5 mol%), the LAC reached the highest values for FBN5. In contrast, the LAC values dropped to lower levels for the FBN20 glass sample with 20 mol% of the Fe<sub>2</sub>O<sub>3</sub>. The LAC values decreased in ranges 2.14–0.19 cm<sup>-1</sup> and 0.946–0.19 cm<sup>-1</sup> for glass samples FBN5 and FBN20 at gamma photon energies ranging between 0.184 and 1.408 MeV, respectively. The LAC was moderately reduced with the increasing Fe<sub>2</sub>O<sub>3</sub> contents to the FBN glasses. This decrease is due to the direct proportion of the CS cross-section with the *Z*<sub>eff</sub> ( $\sigma_{com} \propto Z_{eff}$ ).

The MAC is calculated based on the simulated data from the MCNP-5 code and XCOM software program. The difference between the simulated and calculated MAC was calculated using Eq. (16) and tabulated in Table 4. The diff (%) was found lower than 8% for all studied FBN glasses.

$$\text{Diff}(\%) = \frac{[(\mu_m)_{mcnp} - (\mu_m)_{xcom}]}{(\mu_m)_{mcnp}} \times 100 \tag{16}$$

The investigated glass samples’ mass attenuation coefficient (for examples, FNB5 and FNB 20) was compared to some experimental measurements for previously fabricated Bi<sub>2</sub>O<sub>3</sub> and PbO-based glass at gamma photon energy 0.662 MeV, as shown in Fig. 6. The Bi<sub>2</sub>O<sub>3</sub>-based glass was represented by Bi30 and Bi70 reported by Kaewkhao et al., [41], and the PbO-based glass represented by Pb5 and Pb55 fabricated by Limkitjaroenporn et al., [42]. Moreover, the comparison was extended to include the commercial glass samples(RS 253, RS 253 G18, RS 323 G19, RS 360, and RS 520) fabricated by SCHOTT AG [43]. Figure 6 depicts that the investigated glass sample

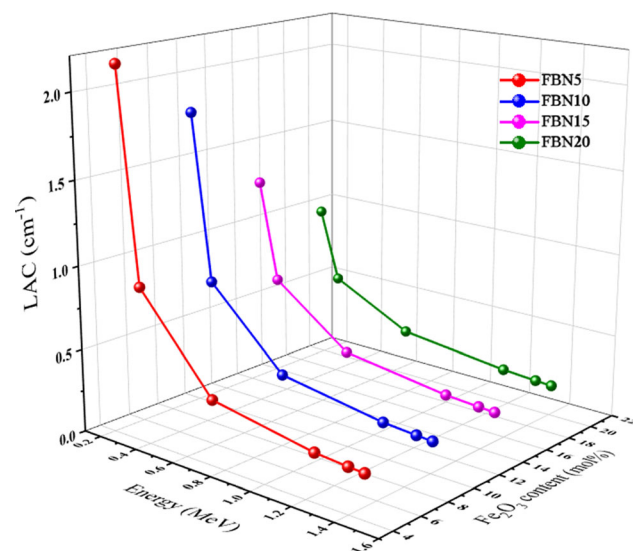


**Fig. 4** The Poisson ratio ( $\sigma$ ) and the micro-hardness (*H*) of the fabricated glass samples at different Fe<sub>2</sub>O<sub>3</sub> substitution ratio

**Table 3** Comparison between the elastic properties of the studied FBN5, FBN10, FBN20, and some previously prepared glass systems

Sample code	Composition (mole fraction)	Density (g cm <sup>-3</sup> )	E (GPa)	B (GPa)	S (GPa)	L (GPa)
FBN5 (present work)	0.75Li <sub>2</sub> B <sub>4</sub> O <sub>7</sub> , 0.2Bi <sub>2</sub> O <sub>3</sub> , 0.05Fe <sub>2</sub> O <sub>3</sub>	3.757	57.67	33.47	23.77	65.17
FBN10 (present work)	0.75Li <sub>2</sub> B <sub>4</sub> O <sub>7</sub> , 0.15Bi <sub>2</sub> O <sub>3</sub> , 0.1Fe <sub>2</sub> O <sub>3</sub>	3.706	65.01	40.93	26.32	76.02
FBN20 (present work)	0.75Li <sub>2</sub> B <sub>4</sub> O <sub>7</sub> , 0.05Bi <sub>2</sub> O <sub>3</sub> , 0.2Fe <sub>2</sub> O <sub>3</sub>	3.587	85.29	65.49	33.24	109.81
G1 [36]	(0.15Bi <sub>2</sub> O <sub>3</sub> ,0.15MoO <sub>3</sub> ,0.4B <sub>2</sub> ), 0.2 SiO <sub>2</sub> , 0.09 Na <sub>2</sub> O, 0.01Fe <sub>2</sub> O <sub>3</sub>	3.053	71.06	73.11	26.83	108.88
5Ba [37]	0.05BaO, 0.3Bi <sub>2</sub> O <sub>3</sub> , 0.65B <sub>2</sub> O <sub>3</sub>	4.97	68.04	52.29	26.88	84.21
15 [38]	0.6B <sub>2</sub> O <sub>3</sub> , 0.15Bi <sub>2</sub> O <sub>3</sub> , 0.10Na <sub>2</sub> O, 0.1CaO, 0.05Al <sub>2</sub> O <sub>3</sub>	4.218	67.6	53.9	26.2	88.8
10 [39]	0.05Al <sub>2</sub> O <sub>3</sub> , 0.29 Na <sub>2</sub> O, 0.56B <sub>2</sub> O <sub>3</sub> , 0.1Bi <sub>2</sub> O <sub>3</sub>	3.229	92.7	67.6	–	–

FBN0 has a  $\mu_m$  equal to 0.0873 cm<sup>2</sup> g<sup>-1</sup>, which is less than the  $\mu_m$  reported for glass samples Bi70 (0.1024

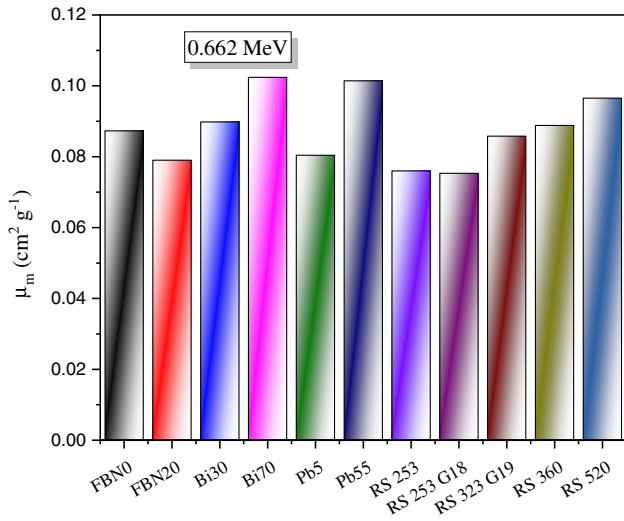
**Fig. 5** The linear attenuation coefficient LAC (cm<sup>-1</sup>) as a function of the energy and the amount of Fe<sub>2</sub>O<sub>3</sub>

cm<sup>2</sup> g<sup>-1</sup>), Pb55 (0.1014 cm<sup>2</sup> g<sup>-1</sup>), and Rs 520 (0.0965 cm<sup>2</sup> g<sup>-1</sup>). In contrast, the FBN0  $\mu_m$  is greater than that reported for glass samples Pb5 (0.0804 cm<sup>2</sup> g<sup>-1</sup>), RS 253 (0.076 cm<sup>2</sup> g<sup>-1</sup>), and RS 253 G18 (0.0753 cm<sup>2</sup> g<sup>-1</sup>). Finally, the  $\mu_m$  for the investigated glass sample FBN0 is convergent with glass samples RS323 G19 (0.0858 cm<sup>2</sup> g<sup>-1</sup>) and RS 360 (0.0888 cm<sup>2</sup> g<sup>-1</sup>).

Figure 7 displays the TF variation of the studied FBN glasses vs. the thickness of the glass at known incoming photon energies (0.184, 0.280, 0.662, 1.173, 1.332, and 1.408 MeV). Two remarkable factors are observed having an effect on TF. The first factor is the incoming photon energy. At low energy (0.180 MeV), the lowest TF values were achieved and decreased from 0.12 to 2.27 E<sup>-05</sup> % for FBN5 glass, while the highest values of TF are decreased from 0.29 to 0.002 % for FBN20 glass. Moreover, at high energy (1.408 MeV), the TF for FBN5 glass was found to decrease from 0.82 to 0.37 % and from 0.83 to 0.38 % for FBN20 glass. A decrease in the wavelength of the gamma photon leads to an increase in the incoming photon energy, which increases the penetration of the

**Table 4** The mass attenuation coefficient of the studied FBN5, FBN10, FBN15, and FBN20 samples

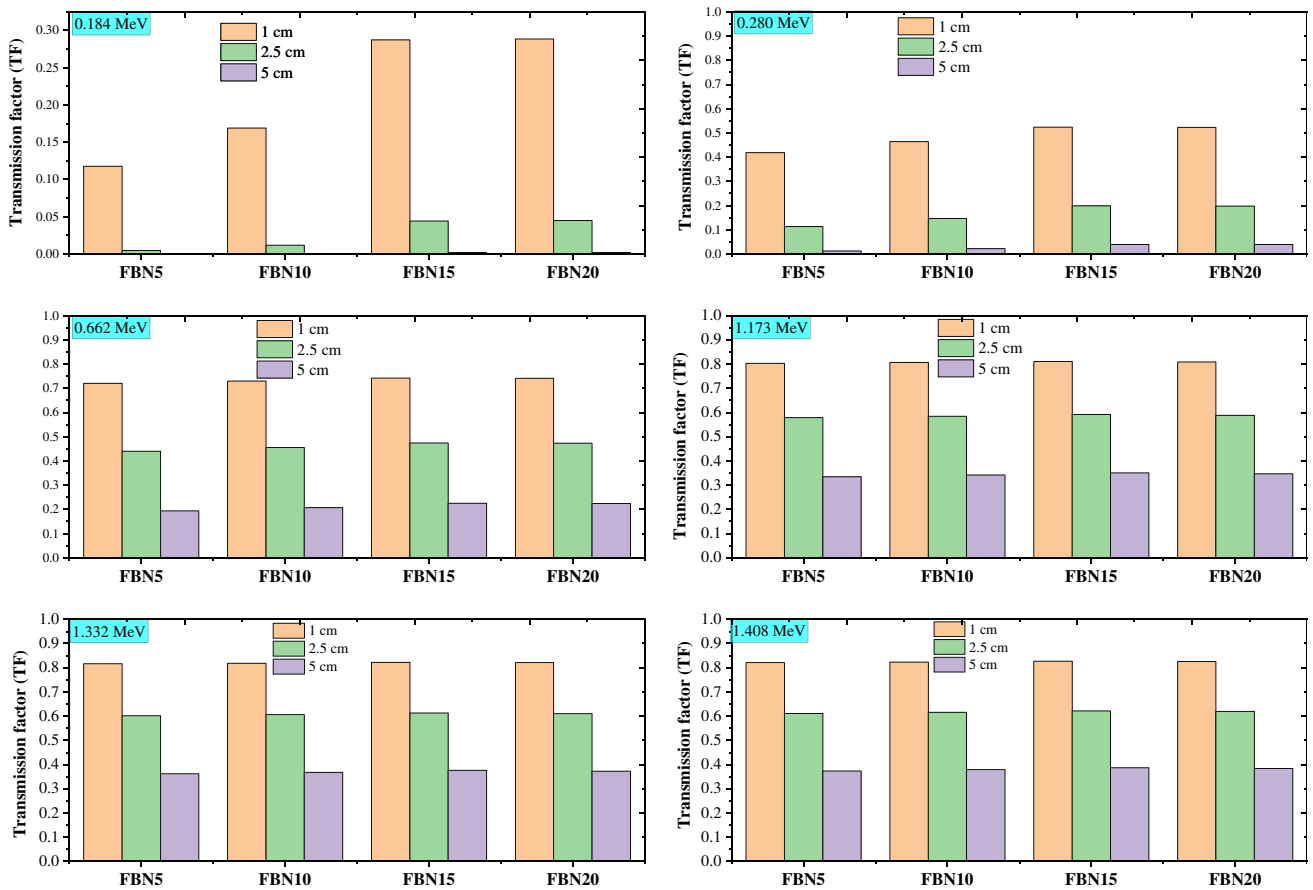
Energy (MeV)	Mass attenuation coefficient (cm <sup>2</sup> g <sup>-1</sup> )											
	FBN 5			FBN10			FBN 15			FBN 20		
	MCNP-5	XCOM	diff (%)	MCNP-5	XCOM	diff (%)	MCNP-5	XCOM	diff (%)	MCNP-5	XCOM	diff (%)
0.184	0.5492	0.5024	8.5163	0.4795	0.4272	10.9084	0.3427	0.3416	0.3222	0.2638	0.2433	7.7625
0.28	0.2319	0.2315	0.1619	0.2073	0.2067	0.2782	0.1779	0.1784	0.3059	0.1456	0.1459	- 0.2202
0.662	0.0873	0.0877	- 0.3790	0.0849	0.0852	- 0.3310	0.0820	0.0823	- 0.2739	0.0788	0.0790	- 0.2009
1.173	0.0582	0.0591	- 1.5189	0.0579	0.0587	- 1.2878	0.0576	0.0582	- 1.0294	0.0573	0.0577	- 0.7237
1.332	0.0541	0.0548	- 1.3051	0.0539	0.0545	- 1.1007	0.0538	0.0542	- 0.8765	0.0536	0.0539	- 0.6228
1.408	0.0525	0.0531	- 1.2346	0.0524	0.0529	- 0.9733	0.0522	0.0526	- 0.7657	0.0521	0.0524	- 0.5371



**Fig. 6** Compares the mass attenuation coefficient of the investigated glass FBN samples with other commercial and previously prepared glass samples

incoming photon power. Therefore, photons’ interactions inside the FBN glasses diminished, and the TF of an incoming photon increased. Second, it was noticed that as the glass thickness increased, the TF decreased. For the investigated glass sample FBN5 at gamma photon energy around 0.184 MeV, the TF reduces from 0.12 to  $2.27 \times 10^{-5}$ , with increasing the glass thickness between 1 and 5, respectively. The reason for this decrease is that the photons required more time to pass the thicker thickness of glass. Thus, more interaction between the material atoms and the gamma photons will be carried out inside the material layers, which causes more resistance for passing the incoming photons. As a result, the TF for the incident photons decreased with increasing the glass thickness.

The half-value layer (HVL) is an another important parameter in the radiation shielding field [44].



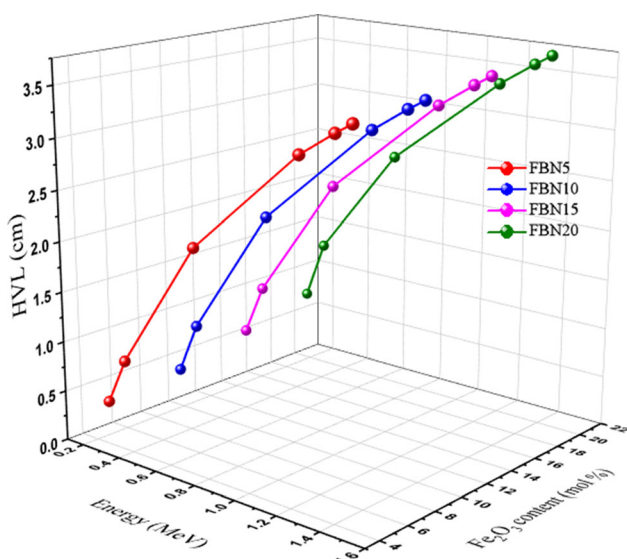
**Fig. 7** The relation between the TF of the FBN samples and the glass thickness between 0.184 and 1.408 MeV



Figure 8 shows that the HVL has an inverse correlation with the LAC, according to Eq. 1. With the increase in incoming photon energy, HVL is quietly increased for different energies. HVL increased from 0.32 to 3.51 cm for FBN5 glasses while it raised from 0.73 to 3.71 cm for FBN20 at photon energies between 0.184 and 1.408 MeV. In the chosen energy range (0.365–1.406 MeV), CS interactions were found to be prevalent, so  $HVL \propto E$ .

This figure (Fig. 8) depicts the simulated HVL affected by  $Fe_2O_3$  content in the FBN glasses. For FBN5 and FBN20, respectively, the HVL rose from 0.32 to 0.73 cm at photon energy 0.184 MeV. It is found at different contents of  $Fe_2O_3$  in the FBN glasses, the molecular weight and density increase. In addition, when LAC and  $Z_{eff}$  increase, the HVL of FBN glasses decreases.

Figure 9 exhibits the variation of  $Z_{eff}$  versus the energy of gamma photon and  $Fe_2O_3$  content. According to the range of gamma energy 0.015–15 MeV, various interactions have been conducted. The photoelectric effect (PE) is the first interaction observed at low photon energies between 0.015 and 1 MeV. Where  $Z_{eff}$ 's values have fallen with the increase in photon energy in the range (0.015–1 MeV), this decrease is due to the cross-section of PE, where  $\sigma_{PE} \propto E^{-3.5}$ . The increase at around 0.080 MeV may reflect Bi K-edge ( $\sim 0.090$  MeV). The second interaction is observed above 0.1 MeV, where the CS is dominant, the estimated values for  $Z_{eff}$



**Fig. 8** The HVL of the studied glasses versus the incoming gamma photon and  $Fe_2O_3$  content

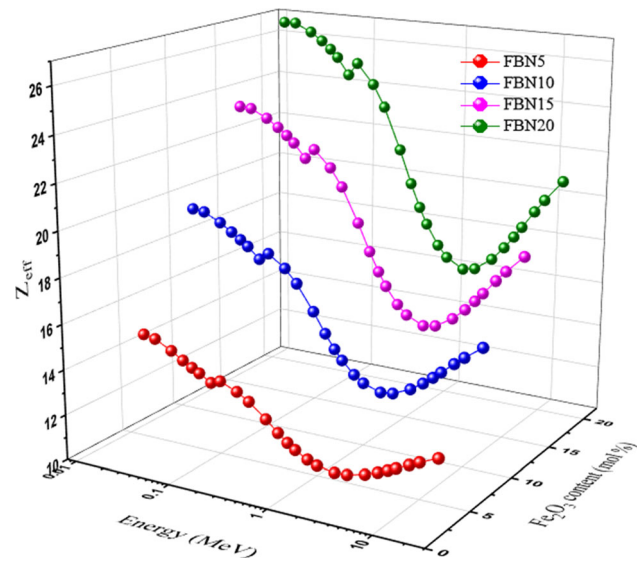


**Fig. 9** The effective atomic number ( $Z_{eff}$ ) of the studied glass samples at various gamma photon energies

reduced progressively with an increase in photon energy. Furthermore, at high gamma energies with several MeV, the pair production (PP) has appeared. The cross-section of PP is  $\sigma_{PP} \propto \log E$ , and  $Z_{eff}$ 's values increased with increasing gamma energy.

The Buildup factors are usually applied to characterize the accumulation of gamma photons. Two main factors are used to explain the passing of gamma photons through the material thickness. These factors are the exposure buildup factor (EBF) and energy absorption buildup factor (EABF). BXCUM program has been used to calculate EBF and EABF for the energies between 0.015 and 15 MeV. Figures 10 and 11 display the EBF and EABF dependence on incoming gamma photon energy, sample penetration depth (PD) in the unit of mfp, and the glass composition. EBF and EABF are affected by the interaction type inside the material. At low photon energies, PE will appear. The incoming photon will interact with the glass material and expel one boundary electron. With increasing the photon energy above 0.1 MeV, the interactions will increase, and the Compton scattering will eject a boundary electron. The rest of the incoming photon energy leads to the accumulation of the scatter photons inside the glass material. Above 2 MeV of incoming photon energies, the accumulation of scattered photons decreases due to the glass material's PP interactions. Thus, the values of EBF and EABF decrease. The highest accumulation factors EBF and EABF

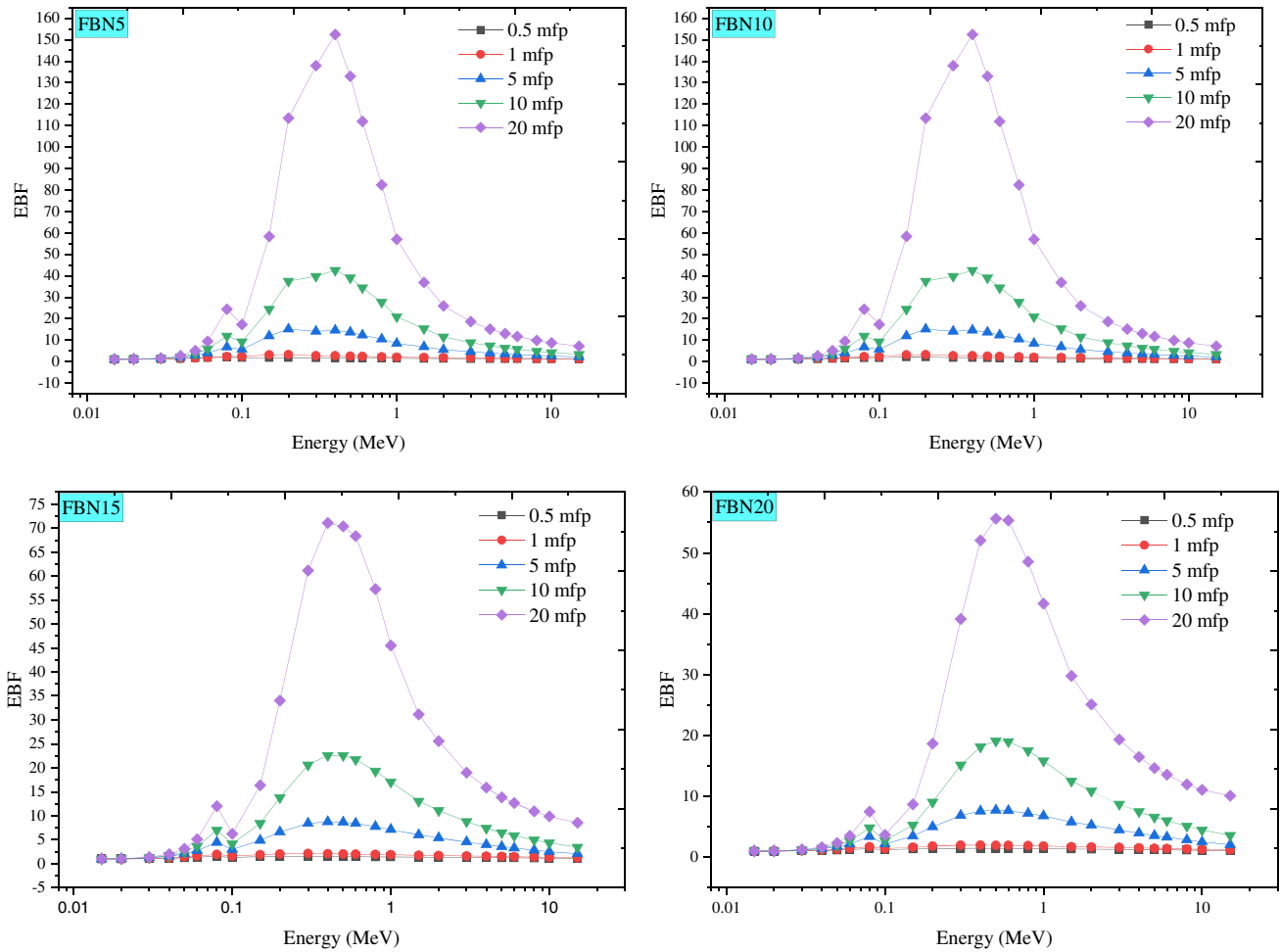


**Fig. 10** The dependence of the exposure buildup factor (EBF) on the photon energy and penetration depth

values in the present FBN glasses are observed at FBN5 and FBN10 related to 5 and 10 mol% of Fe<sub>2</sub>O<sub>3</sub>, respectively. After that, the EBF and EABF values of the FBN glasses decrease gradually with increasing Fe<sub>2</sub>O<sub>3</sub> contents.

The penetration depth (PD) also affects the EBF and EABF values. With increasing the depth of FBN glasses of up to 20 mfp, photons’ accumulation gradually increases. This is due to the photons remaining inside FBN glasses that need more time to penetrate the thickness of FBN glasses; therefore, photons’ accumulation increases. It is achieved with the lowest values of EBF and EABF at low PD (PD = 0.5 mfp) and the highest values at high PD (PD = 20 mfp).

### 4 Conclusion

The molar volume  $V_M$  and the molecular weight  $M_W$  of the FBN glass samples were estimated. The  $V_M$  calculated values decreased from 46.32 to 29.42 cm<sup>3</sup> mol<sup>-1</sup>. The  $M_W$  was reduced from 151.48 to 105.54 g mol<sup>-1</sup>, with an increase in the Fe<sub>2</sub>O<sub>3</sub> insertion ratio between 5 and 20 mol%, respectively. The elastic properties were estimated relying on the Makishima–Mackenzie model. The moduli increased in the range between 57.67–85.29 GPa, 33.47–65.49 GPa, 23.77–33.24 GPa, and 65.17–109.81 GPa for Young, Bulk, Shear, and Longitudinal moduli, respectively. Also, the Poisson’s ratio increased from 0.21 to 0.28, and the micro-hardness improved from 4.55 to 4.81 GPa, raising the Fe<sub>2</sub>O<sub>3</sub> insertion ratio from 5 to 20 MeV. The simulated results depict that the highest LAC achieved at 0.184 MeV decreased from 2.138 to 0.946 cm<sup>-1</sup>, raising the Fe<sub>2</sub>O<sub>3</sub> insertion ratio

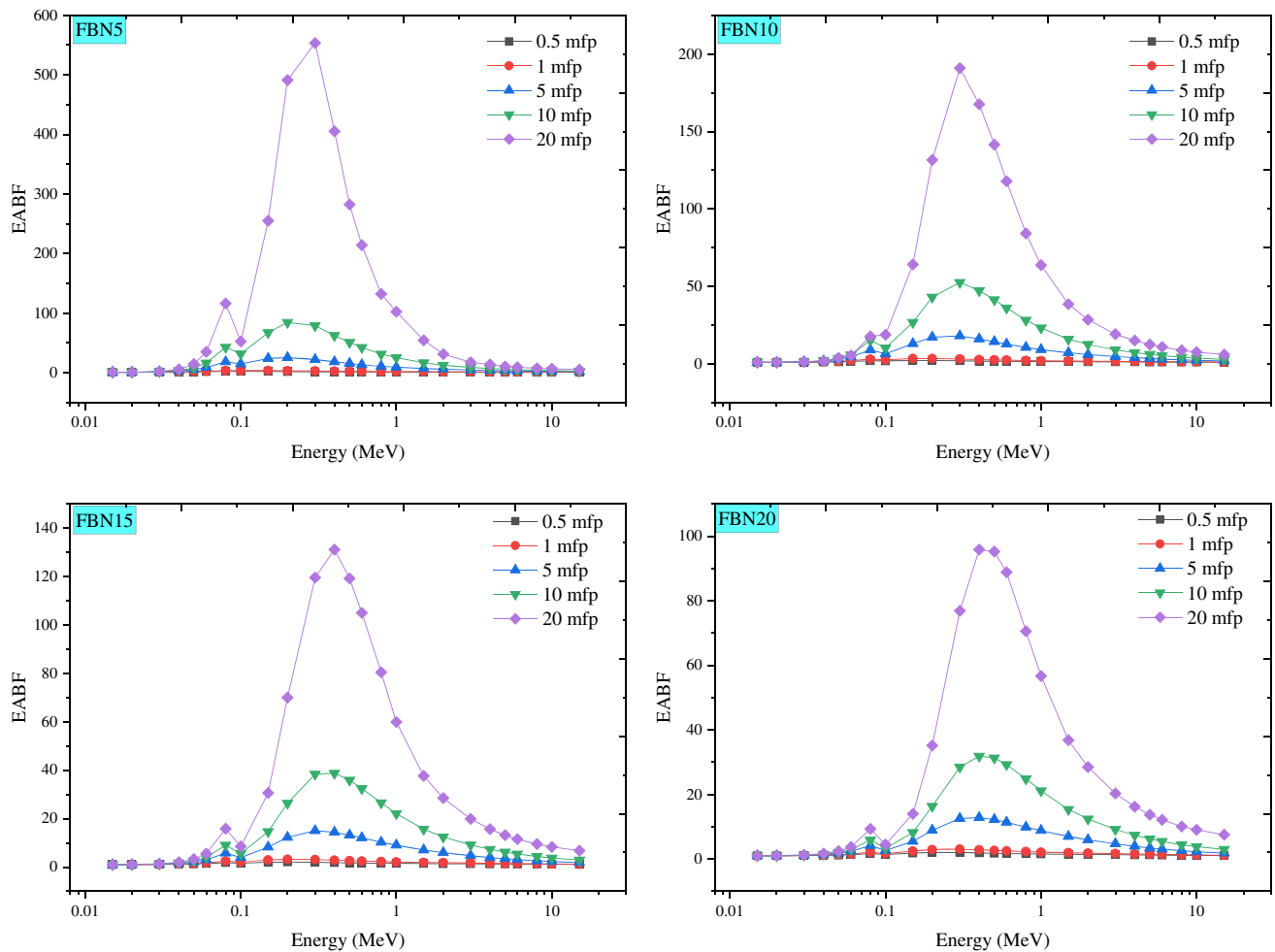


**Fig. 11** The dependence of the energy absorption buildup factor on the gamma photon energy and penetration depth

between 5 and 20 mol%, respectively. The substitution of  $\text{Bi}_2\text{O}_3$  by  $\text{Fe}_2\text{O}_3$  contents reduces the gamma-ray shielding properties of the FBN glass samples and reduces photons' accumulation inside the glass samples (EBF and EABF).

## Acknowledgements

This research was funded by the Deanship of Scientific Research at Princess Nourah bint Abdulrahman University through the Fast-Track Research Funding Program.

## References

1. M.Y. Hanfi, I.V. Yarmoshenko, A.A. Seleznev, G. Malinovsky, E. Ilgasheva, M.V. Zhukovsky, Beta radioactivity of urban surface-deposited sediment in three Russian cities. *Environ. Sci. Pollut. Res.* **27**(32), 40309–40315 (2020)
2. M.H.A. Mhareb, Physical, optical, and shielding features of  $\text{Li}_2\text{O}-\text{B}_2\text{O}_3-\text{MgO}-\text{Er}_2\text{O}_3$  glasses co-doped of  $\text{Sm}_2\text{O}_3$ . *Appl. Phys. A* **126**, 71 (2020)
3. Y.S. Alajerami, D. Drabold, M.H.A. Mhareb, K.L.A. Cimatu, G. Chen, M. Kurudirek, Radiation shielding properties of bismuth borate glasses doped with different concentrations of cadmium oxides. *Ceram. Int.* **46**, 12718–12726 (2020)
4. Q. Chen, K.A. Naseer, K. Marimuthu, P. SuthanthiraKumar, B. Miao, K.A. Mahmoud, M.I. Sayyed, Influence of modifier oxide on the structural and radiation shielding features of  $\text{Sm}^{3+}$ -doped calcium telluro-fluoroborate glass systems. *J. Aust. Ceram. Soc.* (2020). <https://doi.org/10.1007/s41779-020-00531-8>
5. R. Kurtulus, T. Kavas, I. Akkurt, K. Gunoglu, An experimental study and WinXCom calculations on X-ray photon characteristics of  $\text{Bi}_2\text{O}_3$ - and  $\text{Sb}_2\text{O}_3$ -added waste soda-lime-

- silica glass. *Ceram. Int.* **46**(13), 21120–21127 (2020). <http://doi.org/10.1016/j.ceramint.2020.05.188>
6. M. Dong, X. Xue, H. Yang, Z. Li, Highly cost-effective shielding composite made from vanadium slag and boron-rich slag and its properties. *Radiat. Phys. Chem.* **141**, 239–244 (2017)
  7. Y. Al-Hadeethi, M.I. Sayyed, Y.S. Rammah, Fabrication, optical, structural and gamma radiation shielding characterizations of  $\text{GeO}_2\text{-PbO-Al}_2\text{O}_3\text{-CaO}$  glasses. *Ceram. Int.* **46**, 2055–2062 (2020)
  8. I. Akkurt, C. Basyigit, S. Kilincarslan, B. Mavi, A. Akkurt, Radiation shielding of concretes containing different aggregates. *Cement Concr. Compos.* **28**(2), 153–157 (2006)
  9. O.P. Lakhwani, V. Dalal, M. Jindal, A. Nagala, Radiation protection and standardization. *J. Clin. Orthop. Trauma* **10**, 738–743 (2019)
  10. Y. Al-Hadeethi, M.I. Sayyed, H. Mohammed, L. Rimondin, X-ray photons attenuation characteristics for two tellurite based glass systems at dental diagnostic energies. *Ceram. Int.* **46**, 251–257 (2020)
  11. M.Y. Hanfi, M.I. Sayyed, E. Lacomme, I. Akkurt, K.A. Mahmoud, The influence of MgO on the radiation protection and mechanical properties of tellurite glasses. *Nucl. Eng. Technol.* (2020). <https://doi.org/10.1016/j.net.2020.12.012>
  12. N.J. AbuAlRoos, N.A. Baharul Amin, R. Zainon, Conventional, and new lead-free radiation shielding materials for radiation protection in nuclear medicine: a review. *Radiat. Phys. Chem.* **165**, 108439 (2019)
  13. A.M. Zoulfakar, A.M. Abdel-Ghany, T.Z. Abou-Elnasr, A.G. Mostafa, S.M. Salem, H.H. El-Bahnaswy, Effect of antimony-oxide on the shielding properties of some sodium-boro-silicate glasses. *Appl. Radiat. Isot.* **127**, 269–274 (2017)
  14. M. Kurudirek, N. Chutithanapanon, R. Laopaiboon, C. Yenchai, C. Bootjomchai, Effect of  $\text{Bi}_2\text{O}_3$  on gamma ray shielding and structural properties of borosilicate glasses recycled from high pressure sodium lamp glass. *J. Alloys Compd.* **745**, 355–364 (2018)
  15. N. Chanthima, J. Kaewkhao, P. Limsuwan, Study of photon interactions and shielding properties of silicate glasses containing  $\text{Bi}_2\text{O}_3$ , BaO, and PbO in the energy region of 1 keV to 100 GeV. *Ann. Nucl. Energy* **41**, 119–124 (2012)
  16. M. Mariyappan, K. Marimuthu, M.I. Sayyed, M.G. Dong, U. Kara, Effect  $\text{Bi}_2\text{O}_3$  on the physical, structural, and radiation shielding properties of  $\text{Er}^{3+}$  ions doped bismuth sodiumfluoroborate glasses. *J. Non-Cryst. Solids* **499**, 75–85 (2018)
  17. Y. Al-Hadeethi, M.I. Sayyed, A comprehensive study on the effect of  $\text{TeO}_2$  on the radiation shielding properties of  $\text{TeO}_2\text{-B}_2\text{O}_3\text{-Bi}_2\text{O}_3\text{-LiF-SrCl}_2$  glass system using Phy-X/PSD software. *Ceram. Int.* **46**, 6136–6140 (2020)
  18. P. Yasaka, N. Pattanaboonmee, H.J. Kim, P. Limkitjaroenporn, J. Kaewkhao, Gamma radiation shielding and optical properties measurements of zinc bismuth borate glasses. *Ann. Nucl. Energy* **68**, 4–9 (2014)
  19. V.P. Singh, N.M. Badiger, J. Kaewkhao, Radiation shielding competence of silicate and borate heavy metal oxide glasses: comparative study. *J. Non-Cryst. Solids* **404**, 167–173 (2014)
  20. K.M. Kaky, M.I. Sayyed, A.A. Ati, M.H.A. Mhareb, K.A. Mahmoud, S.O. Baki, M.A. Mahdi, Germanate oxide impacts on the optical and gamma radiation shielding properties of  $\text{TeO}_2\text{-ZnO-Li}_2\text{O}$  glass system. *J. Non-Cryst. Solids* **546**, 120272 (2020)
  21. Y. Al-Hadeethi, M.I. Sayyed,  $\text{BaO-Li}_2\text{O-B}_2\text{O}_3$  glass systems: potential utilization in gamma radiation protection. *Prog. Nucl. Energy* **129**, 103511 (2020)
  22. A.A. Hendi, M. Rashad, M.I. Sayyed, Gamma radiation shielding study of tellurite glasses containing  $\text{V}_2\text{O}_5$  and  $\text{Bi}_2\text{O}_3$  using Geant4 code. *Int. Ceram.* (2020). <https://doi.org/10.1016/j.ceramint.2020.08.053>
  23. S. Yasmin, B.S. Barua, M.U. Khandaker, M.A. Rashid, D.A. Bradley, M.A. Olatunji, M. Kamal, Studies of ionizing radiation shielding effectiveness of silica-based commercial glasses used in Bangladeshi dwellings. *Results Phys.* **9**, 541–549 (2018)
  24. W. Rachniyom, W. Chaiphaksa, P. Limkitjaroenporn, S. Tuschaoen, N. Sangwanatee, J. Kaewkhao, Effect of  $\text{Bi}_2\text{O}_3$  on radiation shielding properties of glasses from coal fly ash. *Mater. Today* **5**, 14046–14051 (2018)
  25. Y. Al-Hadeethi, M.I. Sayyed, Radiation attenuation properties of  $\text{Bi}_2\text{O}_3\text{-Na}_2\text{O-V}_2\text{O}_5\text{-TiO}_2\text{-TeO}_2$  glass system using Phy-X/PSD software. *Ceram. Int.* **46**, 4795–4800 (2020)
  26. Y.S. Rammah, F.I. El-Agwany, K.A. Mahmoud, A. Novatski, R. El-Mallawany, Role of ZnO on  $\text{TeO}_2\text{-Li}_2\text{O-ZnO}$  glasses for optical and nuclear radiation shielding applications utilizing MCNP5 simulations and WINXCOM program. *J. Non-Cryst. Solids* **544**, 120162 (2020)
  27. M.I. Sayyed, Y. Al-Hadeethi, M.M. AlShammari, M. Ahmed, S.H. Al-Heniti, Y.S. Rammah, Physical, optical and gamma radiation shielding competence of newly borotellurite based glasses:  $\text{TeO}_2\text{-B}_2\text{O}_3\text{-ZnO-Li}_2\text{O}_3\text{-Bi}_2\text{O}_3$ . *Ceram. Int.* **47**, 611–618 (2021)
  28. A. Al-Hajry, N. Tashtoush, M.M. El-Desoky, Characterization and transport properties of semiconducting  $\text{Fe}_2\text{O}_3\text{-Bi}_2\text{O}_3\text{-Na}_2\text{B}_4\text{O}_7$  glasses. *Phys. B* **368**, 51–57 (2005)
  29. S. Inaba, S. Fujino, K. Morinaga, Young's modulus and compositional parameters of oxide glasses. *J. Am. Ceram. Soc.* **82**(12), 3501–3507 (1999)
  30. A. Makishima, J.D. Mackenzie, Direct calculation of Young's modulus of glass. *J. Non-Cryst. Solids* **12**, 35–45 (1973)

31. A. Makishima, J.D. Mackenzie, Calculation of Bulks modulus, Shear modulus and Poisson's ratio of glass. *J. Non-Cryst. Solids* **17**, 147–157 (1975)
32. X-5 Monte Carlo Team, MCNP-A General Monte Carlo N-Particle Transport Code, Version 5, Los Alamos Controlled Publication. LA-CP-03-0245 (2003)
33. F. Akman, R. Durak, M.F. Turhan, M.R. Kaçal, Studies on effective atomic numbers, electron densities from mass attenuation coefficients near the Kedge in some samarium compounds. *Appl. Radiat. Isot.* **101**, 107–113 (2015)
34. E.A. AbdelWahab, M.S.I. Koubisy, M.I. Sayyed, K.A. Mahmoud, A.F. Zatsepin, S.A. Makhlof, Kh.S. Shaaban, Novel borosilicate glass system:  $\text{Na}_2\text{B}_4\text{O}_7\text{-SiO}_2\text{-MnO}_2$ : synthesis, average electronics polarizability, optical basicity, and gamma-ray shielding features. *J. Nanocryst. Solids* **553**, 120509 (2021)
35. Ö. Eyecioğlu, A.M. El-Khayatt, Y. Karabul, M. Çağlar, O. Toker, O. İçelli, BXCUM: a software for computation of radiation sensing. *Radiat. Eff. Defects Solids* **174**, 506–518 (2019)
36. S.A.M. Issa, M. Ahmad, H.O. Tekin, Y.B. Saddeek, M.I. Sayyed, Effect of  $\text{Bi}_2\text{O}_3$  content on mechanical and nuclear radiation shielding properties of  $\text{Bi}_2\text{O}_3\text{-MoO}_3\text{-B}_2\text{O}_3\text{-SiO}_2\text{-Na}_2\text{O-Fe}_2\text{O}_3$  glass system. *Results Phys.* **13**, 102165 (2019)
37. M.I. Sayyed, S.A.M. Issa, H.O. Tekin, Y.B. Saddeek, Comparative study of gamma-ray shielding and elastic properties of  $\text{BaO-Bi}_2\text{O}_3\text{-B}_2\text{O}_3$  and  $\text{ZnO-Bi}_2\text{O}_3\text{-B}_2\text{O}_3$  glass systems. *Mater. Chem. Phys.* **217**, 11–22 (2018)
38. R. El-Mallawany, H.A. Afifi, M. El-Gazery, A.A. Ali, Effect of  $\text{Bi}_2\text{O}_3$  addition on the ultrasonic properties of pentatertiary borate glasses. *Measurement* **116**, 314–317 (2018)
39. Y.B. Saddeek, M.A. Azooz, A.B. Saddek, Ultrasonic investigations of some bismuth borate glasses doped with  $\text{Al}_2\text{O}_3$ . *Bull. Mater. Sci.* **38**(1), 241–246 (2015)
40. N. Yıldız Yorgun, E. Kavaz, H.O. Tekin, M.I. Sayyed, Ö.F. Özdemir, Borax effect on gamma and neutron shielding features of lithium borate glasses: an experimental and Monte Carlo studies. *Mater. Res. Express* **6**, 115217 (2019)
41. J. Kaewkhao, A. Pokaipisit, P. Limsuwan, Study on borate glass system containing with  $\text{Bi}_2\text{O}_3$  and  $\text{BaO}$  for gamma-rays shielding materials: comparison with  $\text{PbO}$ . *J. Nucl. Mater.* **399**, 38–40 (2010)
42. P. Limkitjaroenporn, J. Kaewkhao, P. Limsuwan, W. Chewpraditkul, Physical, optical, structural, and gamma-ray shielding properties of lead sodium borate glasses. *J. Phys. Chem. Solids* **72**, 245–251 (2011)
43. SCHOTT AG, [http://www.schott.com/advanced\\_optics/english/products/optical-materials/special-materials/radiation-shielding-glasses/index.html](http://www.schott.com/advanced_optics/english/products/optical-materials/special-materials/radiation-shielding-glasses/index.html)
44. M. Dong, X. Xue, H. Yang, D. Liu, C. Wang, Z. Li, A novel comprehensive utilization of vanadium slag: as gamma ray shielding material. *J. Hazard. Mater.* **318**, 751–757 (2016)

**Publisher's Note** Springer Nature remains neutral with regard to jurisdictional claims in published maps and institutional affiliations.